

# Doping-dependent orbital magnetism in Chromium pnictides

Henri G. Mendonça

*Instituto de Física, Universidade Federal de Uberlândia, Uberlândia, Minas Gerais, 38400-902, Brazil*

George B. Martins

*Instituto de Física, Universidade Federal de Uberlândia, Uberlândia, Minas Gerais, 38400-902, Brazil*

Lauro B. Braz

*Instituto de Física, Universidade de São Paulo, São Paulo, São Paulo, 05508-090, Brazil*

---

## Abstract

We present results for the phase diagram of the parent compound LaCrAsO under electron doping using the matrix random-phase approximation. At low doping levels, the system stabilizes an antiferromagnetic state in which different Cr sublattices carry opposite spins, consistent with experimental observations. As the doping concentration increases, a stripe-type antiferromagnetic phase becomes favored. At even higher doping, the system repeats the two former magnetic states, but with incommensurate magnetic ordering vectors. The commensurate magnetic phases are associated with more localized electrons in the Cr  $d_{3z^2-r^2}$  orbital, whereas the incommensurate phases are linked to the  $d_{xy}$  orbital, whose stronger overlap favors itinerant-electron magnetism.

---

## 1. Introduction

The phase diagram of cuprate superconductors has, since the early days, clearly shown that electron correlations decrease with hole doping (HD), going from the pseudo-gap strange-metal underdoped region to the normal-metal overdoped region, passing through the intermediate optimal-doping maximum- $T_c$  region [1]. Something similar occurs on the electron doping (ED) side of the phase diagram, despite some differences in relation to the HD side: the ED side has lower

$T_c$ 's, the superconducting (SC) phase spans a much narrower doping range, and a spin-density-wave description of the normal metallic state (near optimal doping), treated at the mean-field level, offers a good description of quite a few experimental results (for details, see Armitage *et al.* [2]). One of the possible explanations for these differences is that correlations are weaker in the ED side. Sitting in the middle of the HD and ED regions is a half-filling (zero-doping) antiferromagnetic (AF) Mott-insulator. The many similarities between cuprates and Iron-superconductors (Fe-SC) have lead, since the discovery of the latter, to efforts to find a way of placing under the same umbrella the phase diagrams of both materials. An interesting work by Ishida and Liebisch [3] pointed out that if one defines the Fe-SC doping concentration ( $\delta = n/5 - 1$ ) not in relation to  $n = 6$  ( $\text{Fe}^{2+}$ ), but in relation to the half-filled  $n = 5$  configuration, in the range  $0 \leq \delta \lesssim 0.4$  Fe-SC and cuprates display the same sequence of phases, namely, Mott-insulator/non-Fermi-liquid (bad-metal)/Fermi-liquid, which occur roughly at the same concentration intervals [4], with the parent compound  $\text{LaFeAsO}$  ( $\delta = 0.2$ ) sitting at the boundary between the non-Fermi-liquid and Fermi-liquid phases.

The insight described in Ref. [3] rests on a comparison of ED for Fe-SC with HD for the cuprates. As pointed out in Refs. [5, 6, 7], if one presses the analogy further, it is expected that a possible SC phase obtained by *hole-doping* a putative Fe-SC Mott-insulating phase (i.e., starting from  $n = 5 \equiv \delta = 0$ ) may result in higher  $T_c$  values, as is the case for the cuprates [8]. Given the large number (5) of active  $3d$  orbitals in the Fe-SC, a wide range of variation in  $\delta = n/5 - 1$  requires a large variation in  $n$ . In addition, as the Fe-SC parent compounds already start in the electron doped side of the Mott insulator ( $n = 6 \equiv \delta = 0.2$ ), looking for parent compounds with lower values of  $n$  would be a natural step in reaching the hole-doped side of the phase diagram. The transition metal ions to consider would then be Manganese and Chromium. In that respect,  $\text{BaMn}_2\text{As}_2$ , a compound isostructural to  $\text{BaFe}_2\text{As}_2$ , is an AF insulator (checkerboard G-type order,  $T_N = 625$  K [9, 10, 11]), or rather a small band-gap semiconductor with activation energy  $\approx 0.03$  eV [9], where an insulator-to-metal transition occurs with hole doping via the substitution of a few percent of Ba with K [12, 13, 14]. This transition causes only a small suppression of  $T_N$  and of the ordered magnetic moment (which varies between  $S \sim 2$  to  $5/2$ ), suggesting that doped holes interact weakly with the Mn spin system, and therefore, up to now, no superconductivity has been reported in this compound. It has also been found that  $\text{BaMn}_2\text{As}_2$  undergoes an insulator-to-metal transition under pressure of  $\sim 4.5$  GPa [15, 11]. Attempts to grow  $\text{Ba}(\text{Mn}_{1-x}\text{T}_x)_2\text{As}_2$  ( $\text{T} = \text{Cr, Fe, Co, Ni, Cu, Ru, Rh, Pd, Re, and Pt}$ ) and  $\text{BaMn}_2(\text{As}_{1-x}\text{Sb}_x)_2$  were mostly unsuccessful, as the substitution values for the

majority of these compounds does not exceed 0.5% [16]. Pandey *et al.* [13] demonstrated that  $\text{Ba}_{1-x}\text{K}_x\text{Mn}_2\text{As}_2$  becomes a metal with partial substitution of K for Ba, while retaining the crystal and AF structures of  $\text{BaMn}_2\text{As}_2$  and with nearly the same high  $T_N = 625$  K and large ordered moment  $\mu = 3.9\mu_B/\text{Mn}$ . In reality, Lamsal *et al.* [17] have shown that the local moment AF order in  $\text{Ba}_{1-x}\text{K}_x\text{Mn}_2\text{As}_2$  remains robust for doping concentrations up to  $x = 0.4$ . The chemical potential  $\mu$  is nearly independent of  $x$  for  $0 \leq x \leq 0.4$ , while  $T_N$  decreases to 480 K for  $x = 0.4$ .

As to Cr compounds that are isostructural to 122 Fe-SC, we have  $\text{BaCr}_2\text{As}_2$ , reported to be an itinerant (metallic) antiferromagnet [18, 19], where DFT calculations have suggested a stronger degree of covalency between Cr-As than between Fe-As in Fe-SC's, maybe explaining why Cr doping of  $\text{BaFe}_2\text{As}_2$  does not result in superconductivity.  $\text{EuCr}_2\text{As}_2$  is a metallic compound [20], in which Nandi *et al.* [21] found, through neutron diffraction, that the  $\text{Cr}^{2+}$  magnetic moment ( $1.7\mu_B$ ) have AF G-type order along the c-axis at a very high transition temperature ( $T_N \sim 680$  K). In addition, the  $\text{Eu}^{2+}$  ions are found to order ferromagnetically at  $T_C = 21$  K [21], with a negative magnetoresistance observed below  $T_C$ . The independent magnetic orders in the Cr and Eu layers indicate that they are completely decoupled.

In this work, we present multi-band matrix random-phase approximation calculations for the phase diagram of  $\text{LaCrAsO}$  as a function of electron doping  $n$  in the Cr planes. For doping levels between  $n = 4$  (undoped) and  $n \approx 4.2$ , the system stabilizes an antiferromagnetic (AF) phase in which the Cr sublattices carry opposite spins. At higher doping,  $4.2 \lesssim n \lesssim 4.35$ , a stripe-type AF phase is favored, while further doping induces incommensurate states: AF in the range  $4.35 \lesssim n \lesssim 4.5$  and stripe-type AF for  $n \gtrsim 4.5$ .

Our results reveal two central features of this phase diagram. First, the AF phases with opposite Cr sublattice spins are driven by Fermi-surface changes (Lifshitz transitions). Second, the orbital character of magnetism evolves with doping: at low doping ( $4 \lesssim n \lesssim 4.25$ ), it is dominated by the localized  $d_{3z^2-r^2}$  orbital, whereas at higher doping ( $4.25 \lesssim n \lesssim 4.5$ ), the planar  $d_{xy}$  orbital prevails, marking the crossover from local-moment magnetism to itinerant-electron magnetism.

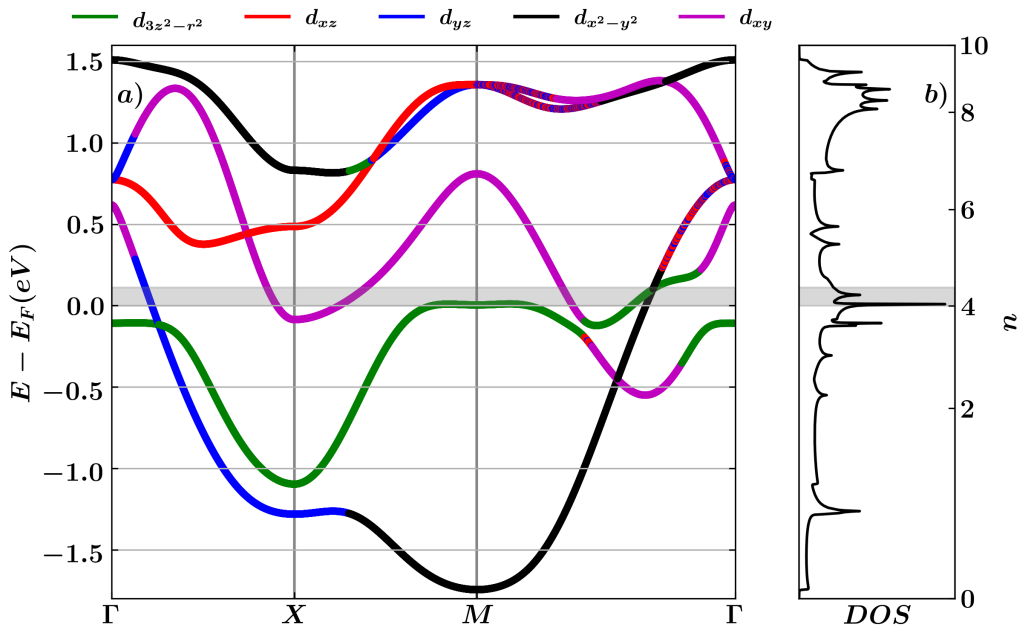


Figure 1: (a) Projected band structure in the  $d$ -orbitals ( $d_{3z^2-r^2}$  in green;  $d_{xz}$  in red;  $d_{yz}$  in blue;  $d_{x^2-y^2}$  in black;  $d_{xy}$  in magenta) of the tight-binding Cr atoms for LaCrAsO along the symmetry lines  $\Gamma - X - M - \Gamma$ . (b) Density of states (DOS) for LaCrAsO. In panels (a) and (b), the grey regions indicate the doping studied in this work ( $n = 4.0 - 4.55$ ).

## 2. Theory

### 2.1. Band structure

The tight-binding electronic Hamiltonian  $H_{\text{TB}}$  describing the low-energy bands of LaCrAsO is given by [7]

$$H_{\text{TB}} = \sum_{\mathbf{k}\sigma\mu\nu} T^{\mu\nu}(\mathbf{k}) d_{\mathbf{k}\mu\sigma}^\dagger d_{\mathbf{k}\nu\sigma}, \quad (1)$$

where  $d_{\mathbf{k}\nu\sigma}$  creates an electron with momentum  $\mathbf{k}$ , spin  $\sigma$ , in an orbital  $\nu$  that is either  $t_{2g}$  ( $xy, zx, yz$ ) or  $e_g$  ( $3z^2 - r^2$  and  $x^2 - y^2$ ). The hopping integrals entering in the expressions for  $T^{\mu\nu}(\mathbf{k})$  can be found in Ref. [7]. They were obtained through a standard downfolding procedure from a full DFT band structure calculation onto a single-chromium tight-binding model [7].

The band structure obtained from the model of Eq. (1) is shown in Fig. 1a), where colors represent the main orbital contributions at each momentum and energy level. Along some high-symmetry directions, the orbital contributions become nearly degenerate and then colors mix in Fig. 1a). Panel b) shows the respective density of states along the full energy resolution of the Wannier model. We highlight the two peaks in the density of states at electron occupations  $n \approx 4.44$  and  $n \approx 4.11$ . These peaks are related to two distinct changes in the Fermi surface topology, also known as a Lifshitz transition. The two transitions are represented on the right-hand side of the panels in Fig. 2. Panels a) and b) represent the first Lifshitz transition, in which an electron pocket around  $(\pi, \pi)$  is lost. The second Lifshitz transition is represented in panels c) and d), where pockets around  $(\pi, 0)$  and  $(\pi/2, \pi/2)$  are turned into large pockets centered at  $(0, 0)$  and  $(\pi, \pi)$ .

Eq. (1) represents a simplified five-band model for the five  $d$  orbitals of Cr. However, in LaCrAsO there is another, inequivalent sublattice site in the square lattice of Cr atoms, which is mapped onto the present Cr  $d$ -orbital model in real space by a  $C_4$  rotation along the  $z$  axis and a  $(\pi, \pi)$  translation in momentum space. This procedure is also called band folding, and it was used to obtain the Fermi surfaces shown on the left-hand side of each panel in Fig. 2. We remark that the first Brillouin zone is changed by this operation, which is shown by black dashed lines. The folded Brillouin zone is related to the unfolded one by a  $C_4$  operation followed by a rescaling of  $1/\sqrt{2}$ .

The total Hamiltonian  $H_T = H_{\text{TB}} + H_{\text{MB}}$  includes, besides  $H_{\text{TB}}$ , also the many-

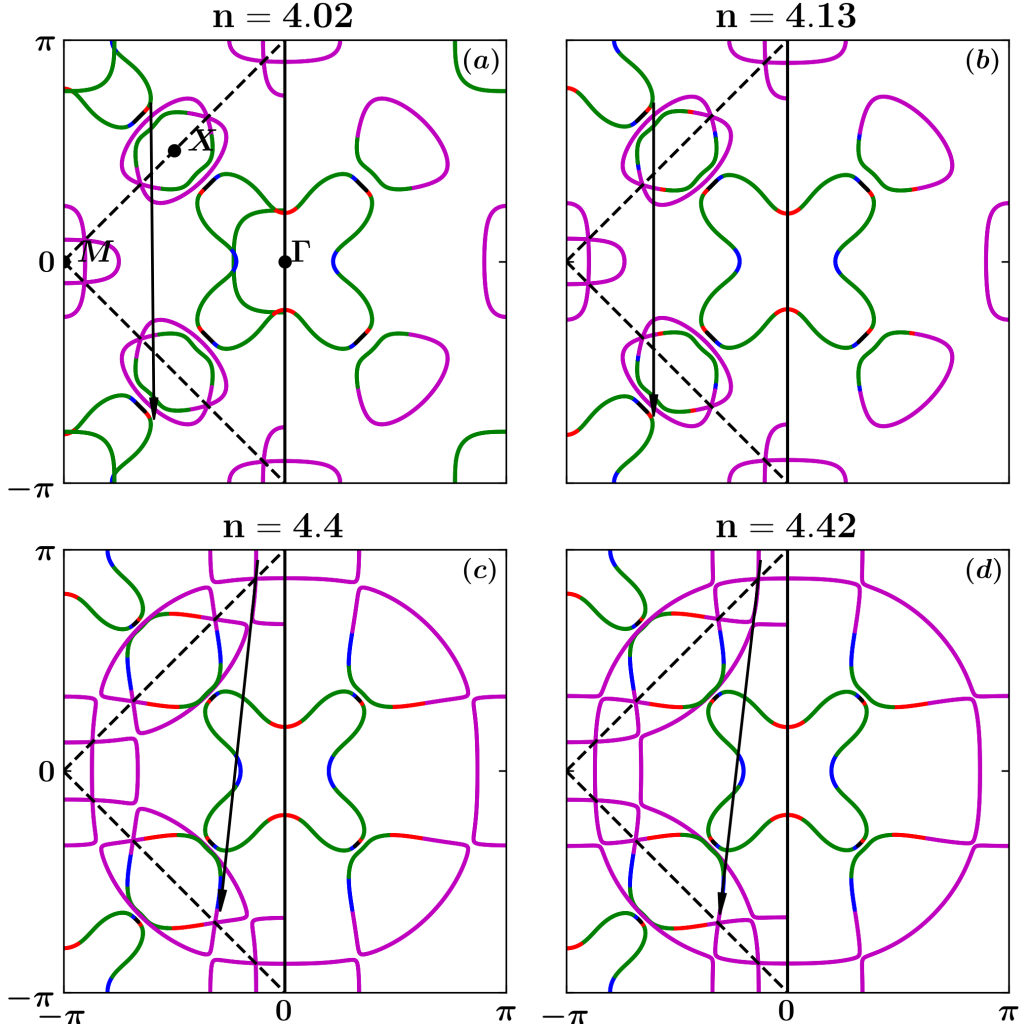


Figure 2: Panels (a) to (d) shows the contribution of the  $d$ -orbitals ( $d_{3z^2-r^2}$  in green;  $d_{xz}$  in red;  $d_{yz}$  in blue;  $d_{x^2-y^2}$  in black;  $d_{xy}$  in magenta) to the Fermi surface pockets for LaCrAsO for  $n = 4.02, 4.13, 4.40, 4.42$ , respectively. For LaCrAsO and in this doping range, the Lifshitz transition occurs between panels (a) and (b), and panels (c) and (d). The nesting vectors are represented by the grey arrows on each of the panels.

body term  $H_{\text{MB}}$ :

$$\begin{aligned}
H_{\text{MB}} = & U \sum_{\mathbf{i}\mu} n_{\mathbf{i}\mu\uparrow} n_{\mathbf{i}\mu\downarrow} + U' \sum_{\mathbf{i}\mu<\nu} n_{\mathbf{i}\mu} n_{\mathbf{i}\nu} \\
& + J \sum_{\mathbf{i}\mu<\nu} (d_{\mathbf{i}\mu\sigma}^\dagger d_{\mathbf{i}\mu\sigma'}^\dagger d_{\mathbf{i}\nu\sigma'} d_{\mathbf{i}\nu\sigma} + h.c.) \\
& + J' \sum_{\mathbf{i}\mu<\nu} (d_{\mathbf{i}\mu\uparrow}^\dagger d_{\mathbf{i}\mu\downarrow}^\dagger d_{\mathbf{i}\nu\downarrow} d_{\mathbf{i}\nu\uparrow} + h.c.),
\end{aligned} \tag{2}$$

where  $\mu, \nu$  denote the Cr  $3d$  orbitals,  $n_{\mathbf{i},\nu}$  is the electron density of orbital  $\nu$  at Chromiun site  $\mathbf{i}$ . The notation is standard and has been described in detail in many publications (see for example Ref. [22]). We will use the usual relations  $U' = U - 2J$ , as well as  $J = J'$ . We are then left with two parameters  $U$  and  $J$ . Following standard procedure, we will fix the ratio  $J/U$ , using  $J = U/4$ , and thus only  $U$  will be left free to vary. Note that the values for the many-body interactions can be substantially smaller than the atomic ones, as they may be screened by bands not included in the Hamiltonian. These many-body terms have been discussed in the literature [23, 22], where more details can be found. Energies are given in electron volts.

## 2.2. Magnetic instabilities

Here, we analyze magnetism and superconductivity in the weak-to-intermediate coupling regime under the matrix random-phase approximation. At low energies, weak-coupling RPA is justified by a parquet renormalization group analysis [24]. Within this framework, an infinite sum of single-scattering momentum  $\mathbf{q}$  Feynman diagrams is performed exactly. It has been shown that both RPA and vertex correction diagrams are taken into account in this approximation [25]. Originating from spin fluctuations, magnetism is analyzed through the Stoner criteria, while superconductivity is studied using an eigenvalue equation for the electron-electron pairing strength as a function of the superconducting gap symmetry.

The bare susceptibility is given by

$$\chi_{st}^{pq}(\mathbf{q}, iv_m) = -\frac{T}{N_{\mathbf{k}}} \sum_{\mathbf{k}} \sum_{i\omega_n} G_{sp}(\mathbf{k}, i\omega_n) G_{qt}(\mathbf{k} + \mathbf{q}, i\omega_n + iv_m), \tag{3}$$

where  $i\omega_n$  ( $iv_m$ ) ar fermionic (bosonic) Matsubara frequencies at temperature  $T$ , the momentum summation is performed over  $N_{\mathbf{k}}$   $\mathbf{k}$ -points, and

$$G_{sp}(\mathbf{k}, i\omega_n) = \sum_{\mu} \frac{a_{\mu}^s(\mathbf{k}) a_{\mu}^{p*}(\mathbf{k})}{i\omega_n - E_{\mu}(\mathbf{k})} \tag{4}$$

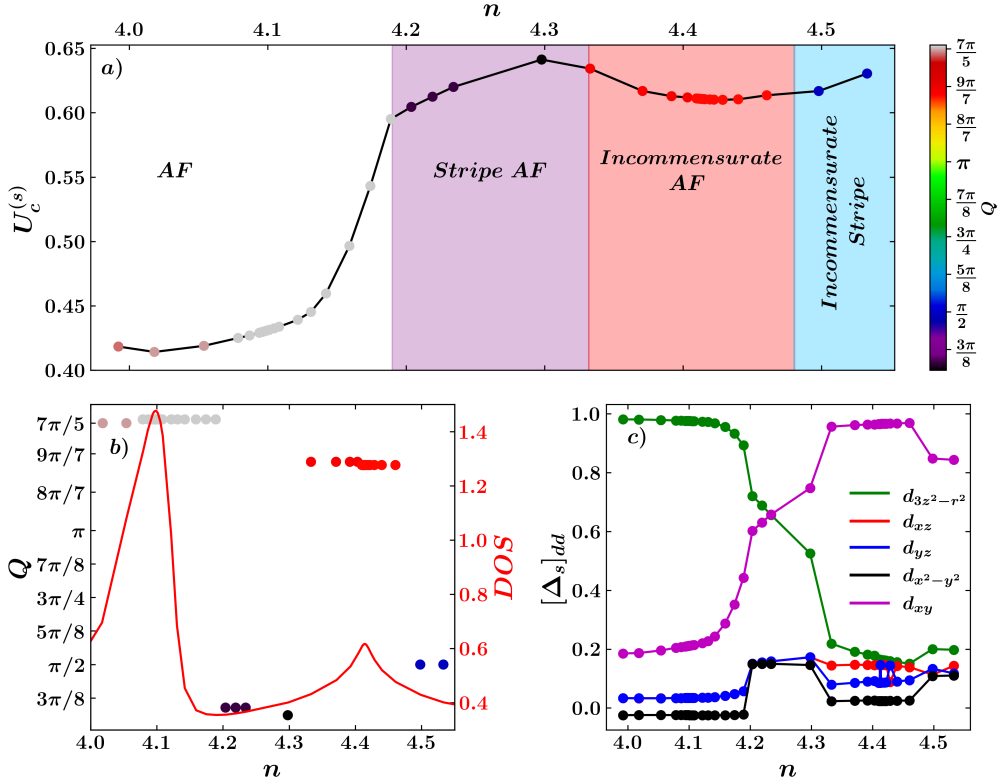


Figure 3: Panels (a) shows the critical Hubbard interaction strength  $U_c^{(s)}$  in the spin channel as a function of electron doping  $n$ . Colors in the scattered points denote the norm of the magnetic ordering vector at the instability  $Q$ . For visualization purposes, we indicate the different magnetic instabilities by colored regions of the diagram. In panel (b), we show the magnetic ordering vector  $Q$  and the density of states as a function of doping. Panel (c) shows the non-zero components of the magnetic order parameter at the instability  $[\Delta_s]_{dd}$  for all orbitals  $d$  for the same electron doping values.

is the non-interacting Green's function for the Hamiltonian  $H_{\text{TB}}$  with eigenvalue  $E_\mu(\mathbf{k})$  and eigenvector elements  $a_\mu^s(\mathbf{k})$ . Here, we perform the Matsubara summation of Eq. (3) using Ozaki method [26].

The RPA spin and charge susceptibilities are given by

$$\hat{\chi}_s(\mathbf{q}, iv_m) = \hat{\chi}_0(\mathbf{q}, iv_m) \left[ \hat{1} - \hat{U}_s \hat{\chi}_0(\mathbf{q}, iv_m) \right]^{-1} \quad (5)$$

$$\hat{\chi}_c(\mathbf{q}, iv_m) = \hat{\chi}_0(\mathbf{q}, iv_m) \left[ \hat{1} + \hat{U}_c \hat{\chi}_0(\mathbf{q}, iv_m) \right]^{-1}, \quad (6)$$

where the interaction matrices  $\hat{U}_{s/c}$  have matrix elements [23]

$$\begin{aligned} (U_s)_{dd}^{dd} &= U, (U_s)_{dd}^{dd} = U', (U_s)_{dq}^{dq} = (U_s)_{qd}^{dq} = J, \\ (U_c)_{dd}^{dd} &= U, (U_c)_{qq}^{dd} = -U' + 2J, (U_c)_{qd}^{dq} = J, (U_c)_{dq}^{dq} = -J + 2U'. \end{aligned} \quad (7)$$

The divergence of the susceptibility denominators imply the eigenvalue equations

$$\alpha_s \hat{1} - \hat{U}_s \hat{\chi}_0(\mathbf{q}, 0) = 0 \quad (8)$$

$$\alpha_c \hat{1} + \hat{U}_c \hat{\chi}_0(\mathbf{q}, 0) = 0. \quad (9)$$

When the eigenvalue  $\alpha_{s/c} = \pm 1$ , the susceptibility diverges marking the onset of a magnetic or charge instability. The eigenvector  $\bar{\Delta}_{s/c}$  corresponding to the leading eigenvalue of Eqs. (5) and (6) carries information on the order parameter at the instability [27]. Reminding that  $J = U/4$  in the present analysis, the onsite Hubbard  $U$  is the only free variable so that we solve Eqs. (8) and (9) for eigenvalues  $\tilde{\alpha}_{s/c}/U_{s/c}^c \equiv \alpha_{s/c}/U$  and simply impose  $\tilde{\alpha}_{s/c} = 1$  to obtain the critical Hubbard interaction  $U_{s/c}^c$ , which is used to probe for the susceptibilities close to the instability. Finally, the magnetic ordering vector  $\mathbf{Q}$  is obtained by the leading eigenvalue of Eqs. (5) and (6) for all  $\mathbf{q}$  within the Brillouin zone. Given the magnetic ordering vector  $\mathbf{Q}$  and the order parameter  $\bar{\Delta}_{s/c}$ , the spin density texture in real space has its periodicity given by the magnetic wave-vector

$$[\bar{\Delta}_s]_{dd}(\mathbf{r}) \equiv [\bar{\Delta}_s]_{dd} e^{-i\mathbf{Q} \cdot \mathbf{r}}. \quad (10)$$

This expression can be simply seen as a Fourier transformation that selects the nesting vector  $\mathbf{Q}$  as having the main weight in momentum space. Finally, in Appendix [Appendix A](#) we show the superconductivity methodology in more detail. We found superconducting gap symmetries as a function of electron doping ranging from the waves  $d_{x^2-y^2}$  to  $d_{xy}$  and then a product of both of them,  $g_{xy(x^2-y^2)}$ .

### 3. Results

The electron-doping  $n$  phase diagram of the present model for LaCrOAs is shown in Fig. 3a), which presents the spin critical Hubbard parameter  $U_s^c$  obtained by solving Eq. (8). The spin fluctuations were found to always be more relevant than the charge fluctuations, with the condition  $U_s^c < U_c^c$  always numerically obtained. The color code in the figure indicates the norm of the nesting vector  $Q = |\mathbf{Q}|$  found for each point in the phase diagram in the folded Brillouin zone view. As a function of doping, the nesting vectors change abruptly revealing a magnetic phase diagram that starts with an AF state, transitioning to an AF stripe, and two distinct SDW states, which we differ by calling them incommensurate AF and incommensurate AF stripe. The critical Hubbard interaction changes very little with doping but still, a plethora of magnetic ordering vectors reveals a strongly doping-dependent magnetic phase diagram.

The norm of nesting vectors  $Q$  is presented in Fig. 3b) along with the density of states profile as a function of electron doping  $n$ . The peaks in the DOS, caused by Lifshitz transitions, coincide with the two major changes in the nesting vectors. These changes have drastic consequences to the orbital contribution within the distinct magnetic states. The matrix elements  $[\bar{\Delta}_s]_{dd}$  of the magnetic order parameter at the instability that is, when  $U = U_s^c$ , are shown as a function of doping  $n$  in Fig. 3c). We note that only the homogeneous elements  $d = q$  are non-zero. Colors indicate the contribution of each orbital for  $[\bar{\Delta}_s]_{dd}$ , where  $d = \{d_{xy}, d_{x^2-y^2}, d_{yz}, d_{xz}, d_{3z^2-r^2}\}$ . At the low-doping region  $n < 4.25$ , the main contribution to the order parameter comes from the  $d_{3z^2-r^2}$  orbital. In fact, the nesting vectors shown in Fig. 2a, b) reveal that nesting connects two FS slices of the same  $d_{3z^2-r^2}$  orbital. On the other hand, Fig. 3b) also shows that at  $n \approx 4.25$  there is a doping region wherein the  $d_{3z^2-r^2}$  and  $d_{xy}$  orbitals closely interplay, and then the  $d_{xy}$  orbital becomes more important for the magnetic order parameter at further doping. The second Lifshitz transition at  $n \approx 4.4$ , as shown in Fig. 2c, d), in fact introduces two new pockets with dominating  $d_{xy}$  contribution and which feature the magnetic nesting.

In Fig. 4, we show the various magnetic patterns in the unfolded unit cell by computing Eq. (10) along the phase diagram of Fig. 3a). In panel a), the AF state is clear in the unfolded unit cell, while panels b-d) show the emergence of the AF stripe. Panel e) shows an AF pattern along the  $(\hat{x} - \hat{y})$  directions of the square lattice, while an incommensurability breaks the periodicity along the  $(\hat{x} + \hat{y})$  direction. The AF pattern along one direction and incommensurability along the other directions motivates labeling this SDW state as an incommensurate

AF instability. Finally, Fig. 4*f*) shows a pattern that resembles the stripe AF of panels *b-d*) but incommensurate, producing wiggly stripes, which motivates labeling the instability incommensurate stripe AF.

#### 4. Discussions

Our findings provide a clear path to understanding the plethora of magnetic phases in  $\text{RCrAsO}$ , where R is a rare earth, as rooted in both Fermi surface topology and orbital specific properties of the electronic states in the vicinity of the Fermi level. This is indeed a general feature of the Fe-SC as suggested by ARPES measurements of Cr- and Mn-substituted  $\text{BaFe}_2\text{As}_2$  showing that doping of electronic states in vicinity of the Fermi level alone does not provide an explanation for the magnetic phase diagram of these materials [28, 29].

Our matrix random-phase approximation calculations based on a DFT-derived tight-binding model shows that charge doping changes the main orbital contribution for the magnetic state of  $\text{RCrAsO}$  from  $d_{3z^2-r^2}$  to  $d_{xy}$ . This trend in the magnetic phase diagram is connected to the orbital contribution to the Fermi surface, where, upon doping, the emergence of a new Fermi surface pocket enhances the  $d_{xy}$  contribution. The Fermi surface topology is the main responsible for the magnetic ordering vector  $\mathbf{Q}$ , which dictates the periodicity of the magnetic texture. In the low doping region, an AF state is predicted, which connects with the dominant  $d_{3z^2-r^2}$  orbital contribution. With doping, the  $d_{3z^2-r^2}$  loses weights at the Fermi surface and the  $d_{xy}$  orbital starts to play a more important role. This intermediate region features a stripe AF state. With further doping, the  $d_{xy}$  orbital dominates, with the appearance of a new Fermi surface sheet, and an incommensurate AF state is followed by incommensurate stripe orders.

The possible overlap between orbitals of neighbor Cr sites in the extended unit cell is favored by the  $xy$ -plane  $d_{xy}$  electrons [30, 31, 32]. In contrast,  $z$ -axis magnetism of the  $d_{3z^2-r^2}$  electrons tends to localize the magnetic spins in the Cr sites. The localized  $d_{3z^2-r^2}$  are then connected with the commensurate AF order, which is perturbed by the overlapping in-plane  $d_{xy}$  orbitals which, eventually, break the Néel-type AF and favor a stripe AF, and further incommensurate orders. Thus, a low-doping localized magnetic picture is suppressed by the electron-doped itinerant-electron magnetism, as proposed in Ref. [32] for iron pnictides.

Electron doping drives a rich landscape to tune magnetism in the Cr-based materials, since electron doping changes Fermi surface properties and the main orbital character of the states contributing to the magnetic order parameter. In this

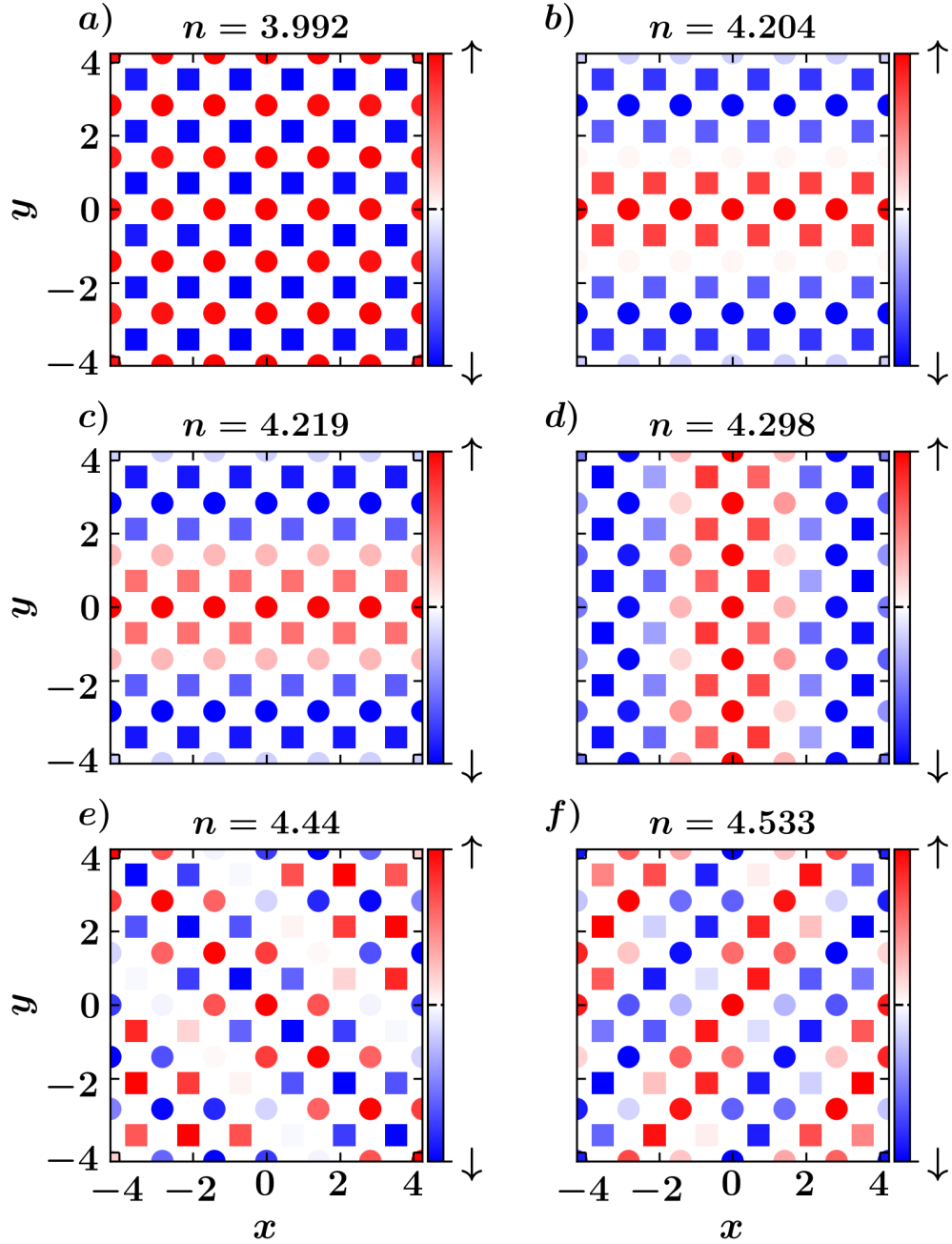


Figure 4: Spin density  $[\bar{\Delta}_s]_{pp}(r)$  mapping the magnetic texture (spin-up: red; spin-down: blue) at Cr sites (Site A: circle; Site B: square) under varying electron doping concentrations:  $n = 3.992$  (panel a),  $n = 4.204$  (panel b),  $n = 4.219$  (panel c),  $n = 4.298$  (panel d),  $n = 4.440$  (panel e), and  $n = 4.533$  (panel f).

direction, adopting  $\text{BaCr}_2\text{As}_2$  as reference compounds, it can also be interpreted that electron doping tunes the magnetism from a localized AF Neél-type phase to an itinerant stripe-type SDW phase in  $\text{BaFe}_2\text{As}_2$ . In terms of the orbital character of the electronic states, Cr substitutions tune the  $d_{3z^2-r^2}$  closer to the Fermi level [28, 33, 34].

We note that the change in orbital hybridizations and the respective symmetries of electronic states in the vicinity of the Fermi surface can be indeed a consequence of charge, hole or electron, doping but not exclusively, as shown for Co- and Mn-substituted  $\text{BaFe}_2\text{As}_2$  [35]. Still, we conjecture that our finding of different magnetic phases associated with each orbital contribution,  $d_{3z^2-r^2}$  or  $d_{xy}$ , is a general result even for a mechanism that is not charge doping. Moreover, our work supports attempts of phase diagrams similar to  $\text{BaCr}_2\text{As}_2$  such as  $\text{Ba}[\text{Cr}_{(1-x)}\text{Fe}_x]_2\text{Cr}_x\text{As}_2$  in search for incommensurate magnetic phases.

### CRediT authorship contribution statement

**Henri G. Mendonça:** Formal Analysis, Visualization, Writing - review and editing. **George B. Martins:** Conceptualization, Writing - review and editing, Formal analysis, Software **Lauro B. Braz:** Conceptualization, Writing - review and editing, Formal analysis, Software.

### Declaration of competing interest

The authors declare that they have no known competing financial interests or personal relationships that could have appeared to influence the work reported in this paper.

### Acknowledgements

The authors are grateful to Maria Calderón, Leni Bascones, Wan-Sheng Wang, Qiang-Hua Wang, and Andrey Chubukov for fruitful discussions on the subject matter of this work. We specially thank Fernando Garcia for a critical review of this work. LBB acknowledges financial support from the São Paulo Research Foundation (FAPESP), Brazil (process number 2023/14902-8), and HPC resources provided by the Superintendency of Information Technology at the University of São Paulo. HGM acknowledges financial support from Coordenação de Aperfeiçoamento de Pessoal de Nível Superior (CAPES) and HPC resources provided by the CENAPAD-SP.

## Appendix A. *d*-wave superconductivity

We probe superconductivity by diagonalizing the Fermi surface-projected integral eigenvalue equation [23]

$$\int_{\text{FS}} dk' \Gamma(\mathbf{k}, \mathbf{k}') \Delta_\alpha(\mathbf{k}') = \lambda_\alpha \Delta_\alpha(\mathbf{k}), \quad (\text{A.1})$$

where  $\Gamma(\mathbf{k}, \mathbf{k}')$  is the kernel function and  $\lambda_\alpha$  (eigenvalues) and  $\Delta_\alpha(\mathbf{k})$  (eigenvectors) are the pairing strength and normalized gap function with symmetry  $\alpha$ . For LaCrOAs, we found symmetries  $\alpha = d_{x^2-y^2}, d_{xy}$ , and  $g_{xy(x^2+y^2)}$ .

According to the matrix-random-phase approximation results, superconductivity in the Cr pnictides could emerge with doping if the Hubbard  $U$  is weak coupling. We show in Fig. 3(a) two horizontal lines demonstrating two possible  $U$  values, for which superconductivity from spin fluctuations can emerge when the  $U < U_s^c$  condition is matched. For  $U < 0.6$  eV, spin fluctuation-driven superconductivity can emerge for the doped compounds, while for  $0.65 < U < 0.6$ , a double-dome structure is predicted.

Fig. A.5 shows the different superconducting gap symmetries found by solving Eq. (A.1) for different filling values. At low doping, the  $d_{x^2-y^2}$  wave is dominating [panel (a)]. However, this symmetry moves to a  $d_{xy}$  wave for mid- $n$  values [panels (b) and (c)] and finally, becomes a  $g_{xy(x^2-y^2)}$  wave [panel (d)] at the high-doping regime.

## References

- [1] P. A. Lee, N. Nagaosa, X.-G. Wen, Doping a Mott insulator: Physics of high-temperature superconductivity, *Rev. Mod. Phys.* 78 (2006) 17. [doi:10.1103/RevModPhys.78.17](https://doi.org/10.1103/RevModPhys.78.17).
- [2] N. P. Armitage, P. Fournier, R. L. Greene, Progress and perspectives on electron-doped cuprates, *Rev. Mod. Phys.* 82 (2010) 2421. [doi:10.1103/RevModPhys.82.2421](https://doi.org/10.1103/RevModPhys.82.2421).
- [3] H. Ishida, A. Liebsch, Fermi-liquid, non-Fermi-liquid, and Mott phases in iron pnictides and cuprates, *Phys. Rev. B* 81 (2010) 054513. [doi:10.1103/PhysRevB.81.054513](https://doi.org/10.1103/PhysRevB.81.054513).
- [4] Note that in this case the cuprates are being hole-doped and the Fe-SC are being electron-doped.

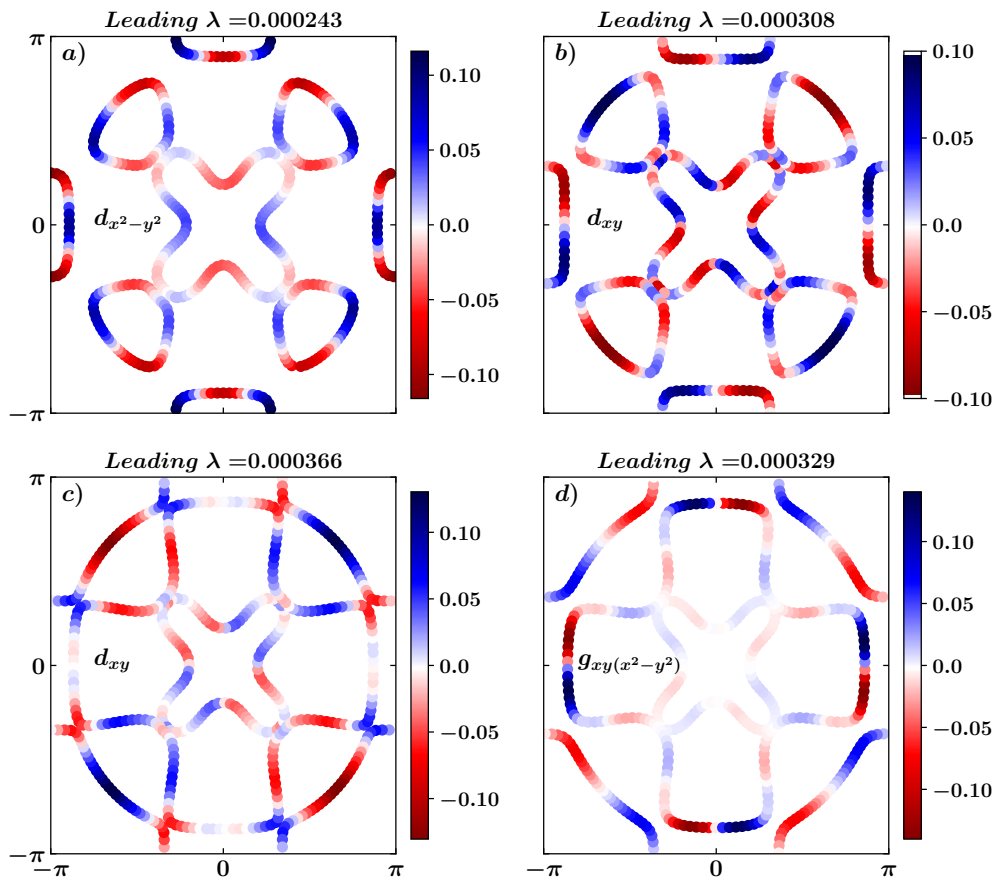


Figure A.5: Superconducting symmetries for different doping levels,  $n = 4.17, 4.30, 4.44, 4.53$  respectively in panels (a) to (d).

[5] J. M. Pizarro, M. J. Calderón, J. Liu, M. C. Muñoz, E. Bascones, Strong correlations and the search for high- $T_c$  superconductivity in chromium pnictides and chalcogenides, Phys. Rev. B 95 (2017) 075115. [doi:10.1103/PhysRevB.95.075115](https://doi.org/10.1103/PhysRevB.95.075115).

[6] M. Edelmann, G. Sangiovanni, M. Capone, L. de' Medici, Chromium analogs of iron-based superconductors, Phys. Rev. B 95 (2017) 205118. [doi:10.1103/PhysRevB.95.205118](https://doi.org/10.1103/PhysRevB.95.205118).

[7] W.-S. Wang, M. Gao, Y. Yang, Y.-Y. Xiang, Q.-H. Wang, Possible superconductivity in the electron-doped chromium pnictide LaOCrAs, Phys. Rev. B 95 (2017) 144507. [doi:10.1103/PhysRevB.95.144507](https://doi.org/10.1103/PhysRevB.95.144507).

[8] Note that, as Cu-doping in  $\text{NaFe}_{1-x}\text{Cu}_x\text{As}$  has been shown to result in electron doping of the FeAs planes [36], changing  $x$  from  $\sim 0.5$  to 0, as done in Ref. [37], is an example of hole-doping a Fe-SC Mott-insulating phase and obtaining a SC phase with a  $T_c^{max} \sim 11.5$  K at  $x = 0.019$  [36], which is not as high as the above reasoning would suggest. However, one may ascribe this not-so-high  $T_c$  to particularities of the Mott-insulating phase in  $\text{NaFe}_{0.52}\text{Cu}_{0.48}\text{As}$  [37].

[9] Y. Singh, A. Ellern, D. C. Johnston, Physical Review B 79 (9) (2009) 094519. [doi:10.1103/PhysRevB.79.094519](https://doi.org/10.1103/PhysRevB.79.094519), [link].  
URL <http://link.aps.org/doi/10.1103/PhysRevB.79.094519>

[10] Y. Singh, M. A. Green, Q. Huang, A. Kreyssig, R. J. McQueeney, D. C. Johnston, A. I. Goldman, Physical Review B 80 (10) (2009) 100403. [doi:10.1103/PhysRevB.80.100403](https://doi.org/10.1103/PhysRevB.80.100403), [link].  
URL <http://link.aps.org/doi/10.1103/PhysRevB.80.100403>

[11] B. S. Jacobs, A. Pandey, `bamn2p2`: Highest magnetic ordering temperature 122-pnictide compound, Phys. Rev. Mater. 7 (2023) 044410. [doi:10.1103/PhysRevMaterials.7.044410](https://doi.org/10.1103/PhysRevMaterials.7.044410).  
URL <https://link.aps.org/doi/10.1103/PhysRevMaterials.7.044410>

[12] J.-K. Bao, H. Jiang, Y.-L. Sun, W.-H. Jiao, C.-Y. Shen, H.-J. Guo, Y. Chen, C.-M. Feng, H.-Q. Yuan, Z.-A. Xu, G.-H. Cao, R. Sasaki, T. Tanaka, K. Matsubayashi, Y. Uwatoko, Weakly ferromagnetic metallic state in heavily doped  $\text{ba}_{1-x}\text{k}_x\text{mn}_2\text{as}_2$ , Phys. Rev. B 85 (2012) 144523. [doi:10.1103/PhysRevB.85.144523](https://doi.org/10.1103/PhysRevB.85.144523)

[PhysRevB.85.144523](#).

URL <http://link.aps.org/doi/10.1103/PhysRevB.85.144523>

- [13] A. Pandey, R. S. Dhaka, J. Lamsal, Y. Lee, V. K. Anand, A. Kreyssig, T. W. Heitmann, R. J. McQueeney, A. I. Goldman, B. N. Harmon, A. Kaminski, D. C. Johnston, Physical Review Letters 108 (8) (2012) 087005. [doi:10.1103/PhysRevLett.108.087005](#), [link].  
URL <http://link.aps.org/doi/10.1103/PhysRevLett.108.087005>
- [14] N. S. Sangeetha, V. Smetana, A.-V. Mudring, D. C. Johnston, [Antiferromagnetism in semiconducting  \$\text{sr}\text{mn}\_2\text{sb}\_2\$  and  \$\text{bamn}\_2\text{sb}\_2\$  single crystals](#), Phys. Rev. B 97 (2018) 014402. [doi:10.1103/PhysRevB.97.014402](#).  
URL <https://link.aps.org/doi/10.1103/PhysRevB.97.014402>
- [15] A. T. Satya, A. Mani, A. Arulraj, N. V. C. Shekar, K. Vinod, C. S. Sundar, A. Bharathi, Physical Review B 84 (18) (2011) 180515. [doi:10.1103/PhysRevB.84.180515](#), [link].  
URL <http://link.aps.org/doi/10.1103/PhysRevB.84.180515>
- [16] A. Pandey, V. K. Anand, D. C. Johnston, Physical Review B 84 (1) (2011) 014405. [doi:10.1103/PhysRevB.84.014405](#), [link].  
URL <http://link.aps.org/doi/10.1103/PhysRevB.84.014405>
- [17] J. Lamsal, G. S. Tucker, T. W. Heitmann, A. Kreyssig, A. Jesche, A. Pandey, W. Tian, R. J. McQueeney, D. C. Johnston, A. I. Goldman, Physical Review B 87 (14) (2013) 144418. [doi:10.1103/PhysRevB.87.144418](#), [link].  
URL <http://link.aps.org/doi/10.1103/PhysRevB.87.144418>
- [18] D. J. Singh, A. S. Sefat, M. A. McGuire, B. C. Sales, D. Mandrus, L. H. Van-Bebber, V. Keppens, [Itinerant antiferromagnetism in bacras2: Experimental characterization and electronic structure](#), Physical Review B 79 (9) (2009) 094429. [doi:10.1103/PhysRevB.79.094429](#).  
URL <http://link.aps.org/doi/10.1103/PhysRevB.79.094429>
- [19] Z. Ning, P. Das, Y. Lee, N. S. Sangeetha, D. L. Abernathy, D. C. Johnston, R. J. McQueeney, D. Vaknin, L. Ke, [Spin dynamics in the itinerant antiferromagnet  \$\text{srcr}\_2\text{as}\_2\$](#) , Phys. Rev. B 111 (2025) 134438. [doi:10.1103/PhysRevB.111.134438](#).  
URL <https://link.aps.org/doi/10.1103/PhysRevB.111.134438>

[20] U. B. Paramanik, R. Prasad, C. Geibel, Z. Hossain, Itinerant and local-moment magnetism in  $\text{eucr}_2\text{as}_2$  single crystals, *Physical Review B - Condensed Matter and Materials Physics* 89 (14) (2014) 1–8. [doi:10.1103/PhysRevB.89.144423](https://doi.org/10.1103/PhysRevB.89.144423).

[21] S. Nandi, Y. Xiao, N. Qureshi, U. B. Paramanik, W. T. Jin, Y. Su, B. Oulad-diaf, Z. Hossain, T. Brückel, *Magnetic structures of the eu and cr moments in  $\text{eucr}_2\text{as}_2$ : Neutron diffraction study*, *Phys. Rev. B* 94 (2016) 094411. [doi:10.1103/PhysRevB.94.094411](https://doi.org/10.1103/PhysRevB.94.094411)  
URL <http://link.aps.org/doi/10.1103/PhysRevB.94.094411>

[22] K. Kubo, *Pairing symmetry in a two-orbital hubbard model on a square lattice*, *Phys. Rev. B* 75 (2007) 224509. [doi:10.1103/PhysRevB.75.224509](https://doi.org/10.1103/PhysRevB.75.224509)  
URL <https://link.aps.org/doi/10.1103/PhysRevB.75.224509>

[23] S. Graser, T. A. Maier, P. J. Hirschfeld, D. J. Scalapino, *Near-degeneracy of several pairing channels in multiorbital models for the fe pnictides*, *New Journal of Physics* 11 (2) (2009) 025016.  
URL <http://stacks.iop.org/1367-2630/11/i=2/a=025016>

[24] R. M. Fernandes, A. V. Chubukov, *Low-energy microscopic models for iron-based superconductors: a review*, *Rep. Prog. Phys.* 80 (2016) 014503. [doi:10.1088/1361-6633/80/1/014503](https://doi.org/10.1088/1361-6633/80/1/014503).  
URL [https://iopscience.iop.org/article/10.1088/1361-6633/80/1/014503/meta?casa\\_token=Xj08PnhuG4oAAAAA:gofMFXJjs9D7SwV90rTULD2loWli2ww0S8hchbMWX0qwjPYXp1iJtes0JMSpZmsFPBZ0AlRiu04E](https://iopscience.iop.org/article/10.1088/1361-6633/80/1/014503/meta?casa_token=Xj08PnhuG4oAAAAA:gofMFXJjs9D7SwV90rTULD2loWli2ww0S8hchbMWX0qwjPYXp1iJtes0JMSpZmsFPBZ0AlRiu04E)

[25] M. Altmeyer, D. Guterding, P. J. Hirschfeld, T. A. Maier, R. Valentí, D. J. Scalapino, *Role of vertex corrections in the matrix formulation of the random phase approximation for the multiorbital Hubbard model*, *Phys. Rev. B* 94 (2016) 214515. [doi:10.1103/PhysRevB.94.214515](https://doi.org/10.1103/PhysRevB.94.214515).  
URL <https://doi.org/10.1103/PhysRevB.94.214515>

[26] T. Ozaki, *Continued fraction representation of the fermi-dirac function for large-scale electronic structure calculations*, *Phys. Rev. B* 75 (2007) 035123. [doi:10.1103/PhysRevB.75.035123](https://doi.org/10.1103/PhysRevB.75.035123)  
URL <https://link.aps.org/doi/10.1103/PhysRevB.75.035123>

[27] L. V. Boehnke, [Susceptibilities in materials with multiple strongly correlated orbitals](#), Ph.D. thesis, Universität Hamburg, dissertation, oral defence: 2014-10-28 (2015).  
 URL <https://ediss.sub.uni-hamburg.de/handle/ediss/6373>

[28] M. R. Cantarino, K. R. Pakuszewski, B. Salzmann, P. H. A. Moya, W. R. d. S. Neto, G. S. Freitas, P. G. Pagliuso, W. H. Brito, C. Monney, C. Adriano, F. A. Garcia, [Incoherent electronic band states in mn-substituted bafe<sub>2</sub>as<sub>2</sub>](#), Phys. Rev. B 108 (2023) 245124. doi:10.1103/PhysRevB.108.245124.  
 URL <https://link.aps.org/doi/10.1103/PhysRevB.108.245124>

[29] M. dos Reis Cantarino, K. R. Pakuszewski, B. Salzmann, P. H. A. Moya, W. R. da Silva Neto, G. S. Freitas, P. G. Pagliuso, C. Adriano, W. H. Brito, F. A. Garcia, [Hole doping and electronic correlations in Cr substituted BaFe<sub>2</sub>As<sub>2</sub>](#), SciPost Phys. 17 (2024) 141. doi:10.21468/SciPostPhys.17.5.141.  
 URL <https://scipost.org/10.21468/SciPostPhys.17.5.141>

[30] X. Chen, J. Qi, D. Shi, Strain-engineering of magnetic coupling in two-dimensional magnetic semiconductor crsite<sub>3</sub>: Competition of direct exchange interaction and superexchange interaction, Phys. Lett. A 379 (2015) 60–63. doi:10.1016/j.physleta.2014.10.042.

[31] Y. Lou, D. Wu, Y. Liao, C. Fang, Y. Pu, J. Xie, A in-plane biaxial strain tunable electronic structures and magnetic properties of fe2c monolayer, J. Magn. Magn. Mater. 563 (2022) 169959. doi:10.1016/j.jmmm.2022.169959.

[32] E. Bascones, B. Valenzuela, M. J. Calderón, Orbital differentiation and the role of orbital ordering in the magnetic state of fe superconductors, Phys. Rev. B 86 (2012) 174508. doi:10.1103/PhysRevB.86.174508.

[33] J. Nayak, K. Filsinger, G. H. Fecher, S. Chadov, J. Minár, E. D. L. Rienks, B. Büchner, S. P. Parkin, J. Fink, C. Felser, Observation of a remarkable reduction of correlation effects in bacr<sub>2</sub>as<sub>2</sub> by arpes, Proc. Natl. Acad. Sci. U.S.A. 114 (47) (2017) 12425–12429. doi:10.1073/pnas.1702234114.

[34] P. Richard, A. van Roekeghem, B. Q. Lv, T. Qian, T. K. Kim, M. Hoesch, J.-P. Hu, A. S. Sefat, S. Biermann, H. Ding, Is **BaCr<sub>2</sub>As<sub>2</sub>** symmetrical to

**BaFe<sub>2</sub>As<sub>2</sub>** with respect to half 3d shell filling?, Phys. Rev. B 95 (2017) 184516. [doi:10.1103/PhysRevB.95.184516](https://doi.org/10.1103/PhysRevB.95.184516).

- [35] A. G. de Figueiredo, M. R. Cantarino, W. R. da Silva Neto, K. R. Pakuszewski, R. Grossi, D. S. Christovam, J. C. Souza, M. M. Piva, G. S. Freitas, P. G. Pagliuso, C. Adriano, F. A. Garcia, [Orbital localization and the role of the fe and as 4p orbitals in bafe<sub>2</sub>as<sub>2</sub> probed by xanes](#), Phys. Rev. B 105 (2022) 045130. [doi:10.1103/PhysRevB.105.045130](https://doi.org/10.1103/PhysRevB.105.045130).  
URL <https://link.aps.org/doi/10.1103/PhysRevB.105.045130>
- [36] A. F. Wang, J. J. Lin, P. Cheng, G. J. Ye, F. Chen, J. Q. Ma, X. F. Lu, B. Lei, X. G. Luo, X. H. Chen, Phase diagram and physical properties of nafe<sub>1-x</sub>cu<sub>x</sub>as single crystals, Phys. Rev. B 88 (2013) 094516. [doi:10.1103/PhysRevB.88.094516](https://doi.org/10.1103/PhysRevB.88.094516).
- [37] Y. Song, Z. Yamani, C. Cao, Y. Li, C. Zhang, J. S. Chen, Q. Huang, H. Wu, J. Tao, Y. Zhu, W. Tian, S. Chi, H. Cao, Y.-B. Huang, M. Dantz, T. Schmitt, R. Yu, A. H. Nevidomskyy, E. Morosan, Q. Si, P. Dai, A Mott insulator continuously connected to iron pnictide superconductors, Nat. Commun. 7 (2016). [doi:10.1038/ncomms13879](https://doi.org/10.1038/ncomms13879).